

IRON LINE REVERBERATION MAPPING WITH CONSTELLATION-X

A. J. YOUNG

Institute of Astronomy, Madingley Road, Cambridge CB3 0HA

AND

C. S. REYNOLDS¹

JILA, University of Colorado, Campus Box 440, Boulder, CO 80309-0440

Draft version April 26, 2024

ABSTRACT

The broad X-ray iron line seen in the spectra of many AGN is thought to originate from the inner regions of the putative black hole accretion disk, and hence provides a rare probe of that central region. In principle, future high throughput X-ray spectrometers should be able to examine the temporal response of this fluorescent line to flares in the X-ray continuum source (which energizes this emission line) — i.e. iron line reverberation mapping will be possible. It has been previously found that there are robust reverberation signatures of the black hole spin, mass and the X-ray flare location above the accretion disk. Here, we simulate observations of a bright Seyfert nucleus with the proposed NASA mission *Constellation-X* and demonstrate the feasibility of detecting these reverberation signatures with this mission. Hence, starting with *XMM* in 1999, and maturing with *Constellation-X* in c2010, iron line reverberation will open a new window on the innermost regions of AGN.

Subject headings: accretion, accretion disks — black hole physics — galaxies: active — galaxies: Seyfert — X-rays: galaxies

1. INTRODUCTION

X-ray spectroscopic observations of Active Galactic Nuclei (AGN) have provided the first direct probe of the innermost regions of black hole accretion disks which are subject to strong-field general relativistic effects. X-ray illumination of the surface layers of the accretion disk produces a strong iron K α fluorescence line (George & Fabian 1991; Matt, Perola & Piro 1991) which is broadened and skewed in a characteristic manner by the Doppler motion of the disk and gravitational redshifting (Fabian et al. 1989; Laor 1991). Observations of Seyfert 1 galaxies by the Advanced Satellite for Cosmology and Astrophysics (*ASCA*) have confirmed the presence of such lines with the expected broad and skewed profiles (Tanaka et al. 1995; Nandra et al. 1997). Alternative mechanisms (i.e. those not involving black hole accretion disks) for the production of such a broad and skewed line profile appear to fail (Fabian et al. 1995).

The X-ray emission from a typical AGN shows significant short timescale variability, with large amplitude changes in flux in hundreds of seconds. This variability is likely to be associated with the activation of new X-ray emitting regions either above the accretion disk or in a disk-hugging corona. These flares produce an ‘echo’ in the form of a fluorescent iron line response from the disk. The line profile depends upon the space-time geometry, the accretion disk structure and the pattern of the X-ray illumination. Given the low count rate of typical AGN in *ASCA*, it is necessary to observe for long periods ($\sim 10^4$ secs) to obtain sufficiently high signal-to-noise to study the Fe K α emission line profile. Such long exposure times include several hundred light crossing times of a gravitational radius ($1GM/c^3 = 500$ secs for a $10^8 M_\odot$ black hole) so that the observed line profile is *time-averaged* and details of any variability are lost, and this lack of a timescale does not allow the black hole mass to be determined. The time-averaged line profiles possess a degeneracy that does not allow the spin parameter of the black hole to be simply determined;

extremely different space-time geometries and illumination patterns may produce almost identical time-averaged line profiles (Reynolds & Begelman 1997), although their absorption effects differ (Young, Ross & Fabian 1998). Detailed time-resolved observations of such emission line variability using the technique of *reverberation mapping* (Blandford & McKee 1982; Stella 1990; Reynolds et al. 1999, hereafter R99) allows the degeneracies mentioned above to be broken. Reverberation mapping has already been used with great success in the optical and UV wavebands, eg. the AGN Watch results on NGC 5548 (Peterson et al. 1999; AGN Watch). R99 have calculated the iron line response as seen by distant observers for a number of scenarios. Their method is outlined below.

The activation of a new X-ray flaring region is approximated by an instantaneous flash from an isotropic point source above the accretion disk, whose location is specified in Boyer-Lindquist coordinates. The accretion disk is assumed to be geometrically thin and confined to the equatorial plane. Whilst the disk may extend out to large radii we are only interested in the line emitting region within ~ 50 Schwarzschild radii ($50R_s = 100GM/c^2$). The disk is divided into two regions, that inside the radius of marginal stability, r_{ms} , where there are no stable circular orbits and material plunges into the black hole, and that outside r_{ms} where material is assumed to follow essentially Keplerian orbits. r_{ms} is a decreasing function of a , the dimensionless angular momentum per unit mass of the black hole, decreasing from $6GM/c^2$ for a Schwarzschild black hole ($a = 0$) to $\sim 1.2GM/c^2$ for a maximally spinning Kerr black hole ($a = 0.998$), assuming that the accretion disk is in a prograde orbit.

The ionization state of the accreting material is determined by considering the ionization parameter $\xi = 4\pi F_x/n_e$, where F_x is the illuminating X-ray flux and n_e is the electron density. Outside r_{ms} the electron density is very large and the disk is ‘cold’, with iron less ionized than Fe XVII. Inside r_{ms} the density drops rapidly as material plunges into the black hole and, if

this region is illuminated, it may become photoionized, which affects the strength of the fluorescence line that is produced. We use the following prescription

1. $\xi < 100$ — cold fluorescence line at 6.4 keV
2. $100 < \xi < 500$ — no line emission due to resonant trapping and Auger destruction of line photons
3. $500 < \xi < 5000$ — a combination of He-like and H-like lines at 6.67 keV and 6.97 keV each with an effective fluorescent yield equal to that for the neutral case
4. $\xi > 5000$ — no line emission since material is completely ionized.

The X-ray efficiency of the source η_x is defined as $\eta_x = L_x/\dot{m}$, where L_x is the X-ray luminosity and \dot{m} is the mass accretion rate. In general, the higher the source efficiency the more highly ionized the material within r_{ms} becomes. This simple model of the accretion disk is sufficient for our purposes.

Photon paths are traced from the flare to compute the illumination pattern on the disk as a function of time, and the corresponding iron line response. The evolution of the line profile as seen by an observer located at a given inclination to the accretion disk is then calculated. The line response to an instantaneous (δ -function) flare is often referred to as the *transfer function*. For further details on the calculation of these transfer functions the reader is referred to R99.

R99 note that transfer functions contain a number of robust indicators of the space-time geometry and the location of the X-ray emitting regions. It is possible to determine the location of the flares, whether they be on or above the accretion disk, on the approaching or receding side of the disk, or along its rotation axis. It is also possible to differentiate between Schwarzschild and maximally spinning Kerr black holes.

In this paper we simulate Constellation X-ray Mission (*Constellation-X*) observations of the iron line response to such X-ray flares using the transfer functions of R99. *Constellation-X* will be the first X-ray observatory with sufficient sensitivity to detect a significant Fe K α line within a light crossing time for nearby bright Seyfert 1 galaxies (the proposed effective area of *Constellation-X* around the iron line energy is about 5 times that of the X-ray Multi-Mirror satellite (*XMM*) which in turn is about 20 times that of *ASCA*).

The aim of this work is to assess the feasibility of detecting the various reverberation signatures described in R99 which will act as probes of the black hole spin and mass. We expand upon an issue raised by R99 and show that a ‘red-ward moving bump’ in the iron line profile is a robust signature of a black hole with spin parameter $a > 0.9$. We also step beyond the single δ -function flare case and examine whether reverberation from realistic multiple flare cases can be disentangled using an instrument such as *Constellation-X*.

2. SIMULATION METHOD

Our simulations are designed to represent the case of a *Constellation-X* observation of an X-ray bright Seyfert 1 galaxy such as MCG–6–30–15 or NGC 3516. These sources show considerable X-ray continuum flux variability on all timescales, with evidence for flares on short timescales (see Fig. 1). Taking parameters for MCG–6–30–15, a typical average continuum

flux in the range 2–10 keV is 6×10^{-3} ph s $^{-1}$ cm $^{-2}$. The average equivalent width of the fluorescent iron line is 300 eV (Tanaka et al. 1995) which corresponds to a 2–10 keV flux of 10^{-4} ph s $^{-1}$ cm $^{-2}$. These figures may be used to estimate the line flux expected for a given continuum flux, assuming the efficiency of conversion of continuum to line photons remains unchanged.

Initially, we assume a continuum level comparable to the average flux of NGC 3516 (1.2×10^{-2} ph s $^{-1}$ cm $^{-2}$) which is constant apart from an instantaneous (δ -function) flare at some time and localized to a point source above the disk. The flare is assumed to have the equivalent of 10000 seconds of continuum flux. This corresponds to a flare lasting 1000 seconds with 10 times the continuum flux or a flare lasting 5000 seconds with twice the continuum flux. The duration of the flare does not significantly influence our results as long as it is relatively short lived, lasting only a few GM/c^3 . Longer flares would result in the transfer functions being blurred over time; a possibility we discuss in section 3.5. We do not specify a particular spectrum for the flare but assume that the fraction of flux from the flare that is converted into line photons is the same as that inferred from the time-averaged spectrum. *Constellation-X* observations of this system, including photon counting statistics, are then simulated using current estimates of this observatory’s (energy dependent) effective area². The line profile was added to a power-law continuum of photon index 2 which was subtracted from the overall simulated data in order to yield a simulated, time-varying, iron line profile.

The mass of the black hole determines the timescale on which reverberation effects occur. For a $10^8 M_\odot$ black hole, for example, the light crossing time of one gravitational radius is $1GM/c^3 = 500$ sec. This is the time period over which we simulate and record individual iron line profiles in order to study the observability of various reverberation effects. For higher mass black holes the reverberation signatures would be more readily observed since longer integration times may be used. The converse is true of lower mass black holes.

3. RESULTS

3.1. Spin parameter

Measuring black hole spin (and, implicitly, testing general relativity in the strong field limit) is one of the main motivations for studying iron line reverberation. If an X-ray flare occurs along the symmetry axis above the accretion disk, the light echo will split into two distinct ‘rings’, one of which propagates outwards to large radii simply due to light travel time, and one which propagates asymptotically towards the horizon. This last feature is due to the progressively more severe relativistic time delays suffered by photons passing close to the black hole. It produces a red-bump in the line profile which moves to lower energies as time goes on. Equivalently, it produces a ‘red-wing’ in the transfer function. Fig. 2 shows simulated transfer functions for values of the spin parameter a between 0–0.99. For these calculations a low source efficiency $\eta_x = 10^{-3}$ was chosen to maximize the region within r_{ms} that may produce highly redshifted fluorescent line emission. A more realistic, higher value of η_x would result in the region within r_{ms} becoming more highly ionized and less able to produce fluorescent line emission (Reynolds & Begelman 1997). The precise shape of

²Effective area curves were obtained from the NASA Goddard Space Flight Center web-page: <http://constellation.gsfc.nasa.gov/www/area.html>

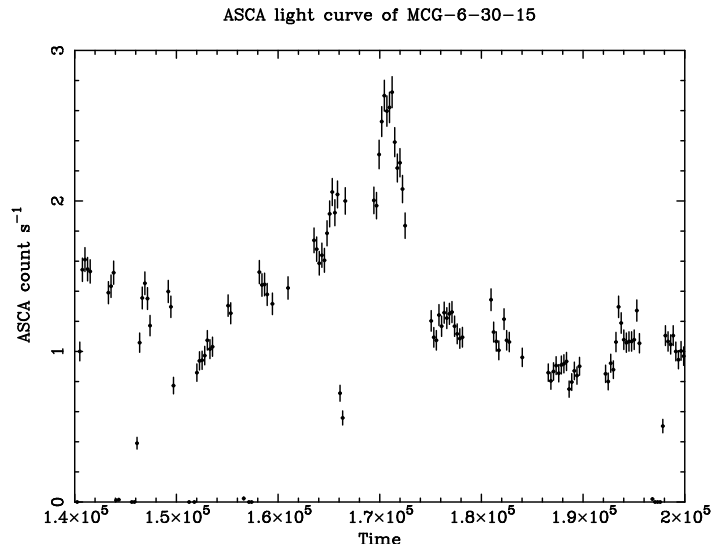


Fig. 1.— 60000 second ASCA light curve of MCG-6-30-15 showing two ‘flares’ lasting a few thousand seconds each (Lee et al 1999).

the ‘red-wing’ depends upon the spin parameter. This red-wing only has a pronounced slope in the case of near-extremal Kerr black holes ($a > 0.9$). Only in these cases will the corresponding line profile possess a red-bump which moves to lower energies as time progresses. We conclude that this feature is a robust signature of near-extremal Kerr black holes.

Fig. 3 shows the line profile in simulated $2GM/c^3$ (1000 s) *Constellation-X* observations of the extreme Kerr case between $23-28GM/c^3$ (11500 s–14000 s) after the flare is observed at time zero. Shown here is the case of a flare on the spin axis of the hole at a height $10GM/c^2$ above the disk plane, viewed almost face-on, at an inclination of 3° . The red bump is clearly seen and its red-ward progress with time is an indicator that emission from around a Kerr black hole is being observed. Thus, this signature is readily observable in such a case.

As the inclination of the observer increases, the photons in the red-wing are distributed over a greater range of energies and times and hence the detectability of the feature is reduced. Fig. 4a shows a simulated transfer function for a disk inclined at 30° around an extreme Kerr black hole. The flare is assumed to be on the symmetry axis at a height of $10GM/c^2$ above the disk plane. Red-tail emission (at ~ 3 keV and $t = 30GM/c^3$) can be discerned above the photon noise. For comparison, Fig. 4b shows the same case but with a Schwarzschild black hole. The differences between the transfer functions are subtle but observable. The data in these figures have been rebinned to increase the signal-to-noise ratio. On the basis of these simulations, we estimate that this phenomenon is observable for source inclinations less than 30° , although the flare location is also an important consideration in determining the observability of this effect.

3.2. Confidence in the determination of the spin parameter

The differences between the theoretical transfer functions for the same source location but different values of the black hole spin parameter may be seen in Fig. 2, the difference between the Schwarzschild, $a = 0$, and nearly maximally spinning Kerr, $a = 0.99$, cases being the most marked. These theoretical transfer functions may be used as templates to fit an observation of

a system inclined at 30° with a flare located $10GM/c^2$ along the rotation axis of the disk. If we simulate an observation with a particular value of a and attempt to fit that simulation with each of the template transfer functions. Fig. 5a shows the results of fitting five simulated observations of the case $a = 0.99$. The $\Delta\chi^2$ values are an indication of the goodness of fit (with a lower $\Delta\chi^2$ representing a better fit), normalized to $\Delta\chi^2 = 0$ at the best fit values. The goodness of fit is seen to improve dramatically as the value of a used in the fit is increased indicating that the black hole is spinning rapidly. Fig. 5b shows a similar plot for of fitting simulated observations of the $a = 0$ case. Again the $\Delta\chi^2$ values are seen to decline sharply towards the best fitting values, and one may conclude that the black hole is not spinning rapidly. In reality a catalogue of transfer functions would be used to fit for different flare locations black hole spin parameters.

3.3. Flare location and the mass of the black hole

The location of the X-ray flares and the mass of the central black hole (i.e. the linear dimensions of the whole system) are also important motivations for performing iron line reverberation mapping of AGN. Ideally, one would take a well-measured iron line response to a large flare and compare it to a library of theoretical transfer functions in order to determine the location of the flare and the mass of the hole (from the time scaling of the transfer function). The multi-dimensional parameter space, coupled with the limitations of realistic data, makes this a challenging problem.

However, there are qualitative features in the transfer functions of R99 that can be used to estimate the mass and flare location. For most flare locations and observer inclinations, there is a re-emergence of the line flux (usually in the red-wing of the line) as the observed echo of the flare works its way round to the back regions of the disk. The time between the initial line response and this re-emergence is $\sim 10 - 20GM/c^3$. Both the initial line response and the re-emergence are easily observable with *Constellation-X* (see Figs. 3, 4b and 6b) for $M \sim 10^8 M_\odot$. Hence masses in this range can be measured to within a factor of two or so. Furthermore, the time between the observed flare

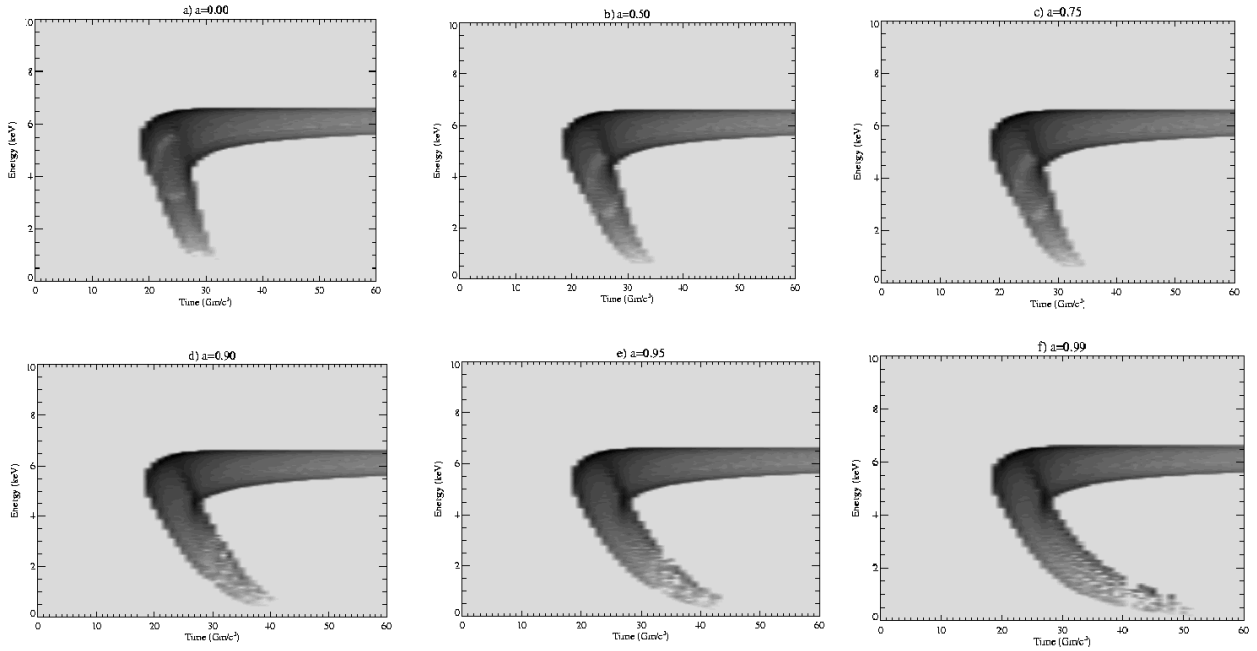


Fig. 2.— Theoretical transfer functions of Fe $K\alpha$ line for different spin parameters, (a) $a = 0$, (b) $a = 0.5$, (c) $a = 0.75$, (d) $a = 0.9$, (e) $a = 0.95$ and (f) $a = 0.99$. The extreme ‘red-tail’ is a robust signature of a rapidly spinning black hole. The flare has been placed on the symmetry axis at a height of $10GM/c^2$ above the disk plane, with an observer inclination of 30° . The source efficiency is $\eta_{\text{sc}} = 10^{-3}$.

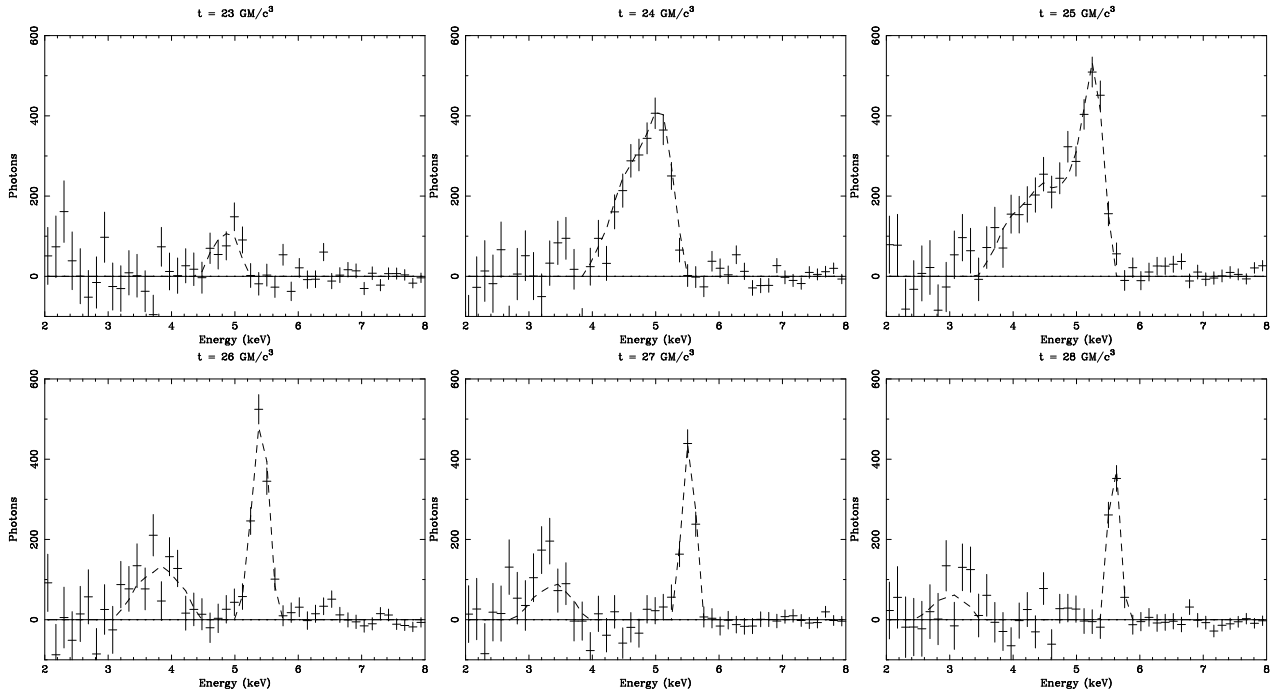


Fig. 3.— $2GM/c^3$ (1000 s) simulated observations of the red-ward moving bump between times $23GM/c^3$ and $28GM/c^3$ for an almost face-on (inclination 3°) accretion disk. The flare occurred on the rotation axis of the hole/disk at a height of $10GM/c^2$ above the disk plane. The red-ward moving bump is a signature of a rapidly spinning black hole. The dashed line shows the theoretical evolution of the line profile.

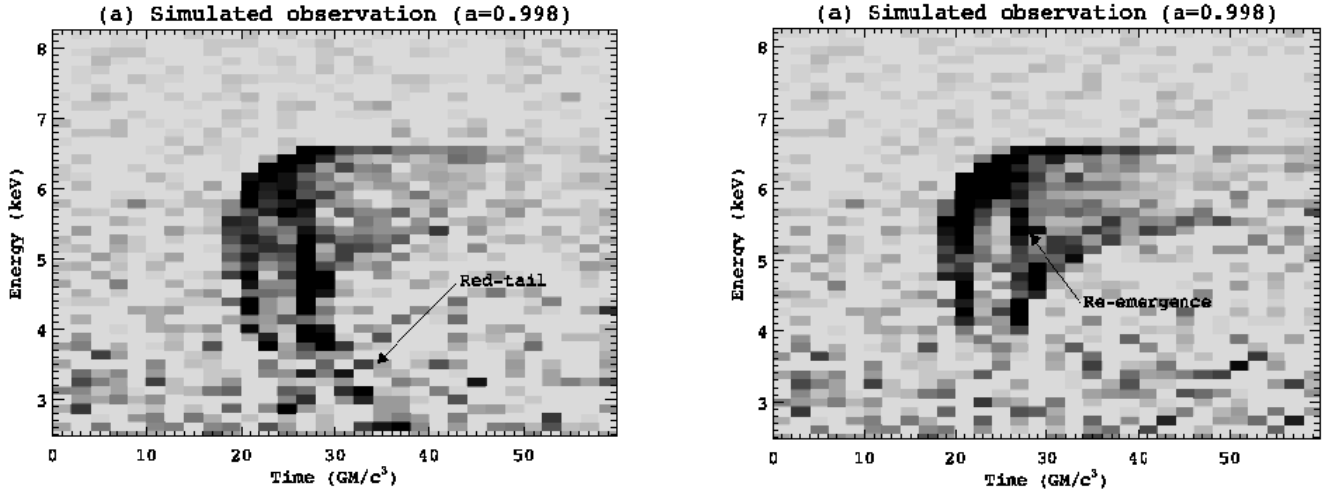


Fig. 4.— Simulated transfer function for (a) an extremal Kerr hole, and (b) a Schwarzschild hole. In both cases, the flare has been placed on the symmetry axis at a height of $10GM/c^2$ above the disk plane, and an observer inclination of 30° has been assumed. The data have been rebinned to produce these figures with improved signal-to-noise ratio.

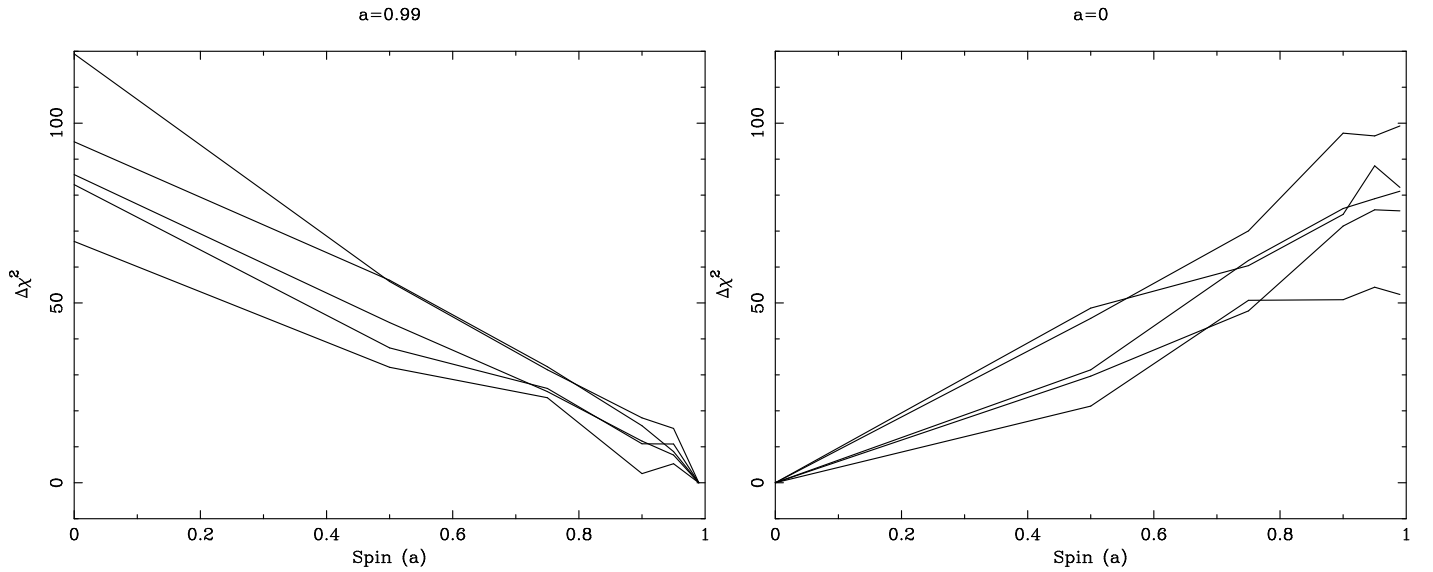


Fig. 5.— Relative goodness of fit to simulated observations with (a) $a = 0.99$ and (b) $a = 0$. $\Delta\chi^2$ decreases with increasing quality of fit. Each line represents an independent simulation.

and the initial line response can be compared with the above time in order to determine if the flare is at high-latitudes above the accretion disk, or in a disk-hugging corona.

3.4. Observing the region within the innermost stable orbit

As matter crosses the innermost stable orbit its radial velocity increases rapidly and its density drops dramatically. If this region of the disk is illuminated by hard radiation, the matter becomes ionized and may emit ‘hot’ iron lines at 6.67 keV and 6.97 keV. In the Schwarzschild case where the innermost stable orbit is at a radius $6GM/c^2$ with a high latitude illuminating source, this results in a high energy ‘loop’ in the transfer function corresponding to the response from this ionized region (Fig. 6; also see Fig. 1(c) and (d) of R99). For an accretion disk at a given inclination the maximum expected blueshift may be calculated and hence, for a ‘cold’ iron line at 6.4 keV, the maximum line energy can be determined. Significant line response at higher energies would be an indication of fluorescence from ionized matter. Our simulations show that these features would be observable by *Constellation-X* for inclined disks around Schwarzschild black holes (see Figs. 6a and 6b). We have simulated a number of observations and by fitting them with two template transfer functions, one with the ‘loop’ and the other without, conclude that the presence of the ‘loop’ is statistically significant. Conversely, the observation of such loops would imply that the innermost stable orbit is some distance from the event horizon which, in turn, would indicate a slowly-rotating black hole.

3.5. More realistic flare models

Considering isolated instantaneous flares is, of course, a great simplification of the complicated activity within the nucleus. Motivated by the light curve of Fig. 1 we consider the slightly more realistic scenario of two overlapping flares in a source with continuum flux comparable to that of MCG–6–30–15. Both flares have a duration of 3000 seconds so each of their transfer functions are smeared over $6GM/c^3$. One is on the approaching side of the disk having the same intensity as the continuum and the other is on the receding side of the disk with twice the intensity of the continuum. The flare on the receding side precedes the flare on the approaching side by $6GM/c^3$. Fig. 7 shows the theoretical line response to this double flare as well as the results of a *Constellation-X* simulation. From the simulated *Constellation-X* data, one can see that there have been two flares and can begin to disentangle the individual transfer functions. The height of the flares above the disk along with their location should be determinable.

It is possible that flares significantly brighter than those simulated here may be observed and the fluorescent responses to

those would be correspondingly stronger. Other galaxies, such as NGC 3516, are twice as bright as MCG–6–30–15 and this would help reduce the error bars associated with the photon statistics. Gravitational focusing of the flare emission towards the disk (Martocchia & Matt 1996) may further pronounce these reverberation signatures for flares occurring extremely close to the black hole, within $\sim 6GM/c^2$. In such cases the observed change in continuum flux would represent only a fraction of the flux incident upon the disk. In addition to the bright flares there will be a background of much smaller flares occurring elsewhere on the disk, the response to which may be approximated by a time-averaged line. These flares will appear as noise in the data.

4. CONCLUSIONS

We have demonstrated that many of the iron line reverberation effects noted by R99 are within reach of *Constellation-X*. In particular, *Constellation-X* will be able to search for the redward moving bump in the iron line profile which is a robust and generic signature of rapidly rotating black holes. Maximally spinning Kerr and Schwarzschild black holes can be discriminated. It will also allow the time delay between a large flare and the iron line response, as well as the form of the corresponding transfer function to be determined. Comparison with a library of computed transfer functions will allow the mass of the hole and the location of the flare to be measured. Although this is a difficult task due to the multi-dimensional parameter space that one must consider, we note that there are easily determinable quantities that allow the black hole mass and flare location to be approximated. The time delay between the initial response and ‘re-emergence’ of the line flux may be used to estimate the black hole mass to within a factor of 2. The time delay between the change in the continuum and the initial response of the iron line, as well as the energy of this response, may be used to estimate the location of the flare. These studies will open up a new, and extremely powerful, probe of the immediate environment of supermassive black holes.

5. ACKNOWLEDGMENTS

We thank Kazushi Iwasawa and Julia Lee for the unpublished recent light curve of MCG–6–30–15, and Andy Fabian for insightful discussion. AJY acknowledges PPARC (UK) for support. CSR acknowledges support from NASA under LTSA grant NAG 5-6337. CSR also acknowledges support from a Hubble Fellowship grant HF-01113.01-98A awarded by the Space Telescope Institute, which is operated by the Association of Universities for Research in Astronomy, Inc., for NASA under contract NAS 5-26555.

REFERENCES

- AGN Watch, <http://www.astronomy.ohio-state.edu/~agnwatch>
 Blandford, R. D., & McKee, C. F. 1982, ApJ, 255, 419
 Fabian, A. C., Rees, M. J., Stellar, L., & White, N. E. 1989, MNRAS, 238, 729
 Fabian, A. C., et al. 1995, MNRAS, 277, L11
 George, I. M., & Fabian, A. C. 1991, MNRAS, 249, 325
 Laor, A. 1991, ApJ, 376, 90
 Lee, J. C., et al. 1999, MNRAS, Submitted
 Martocchia, A., & Matt, G. 1996, MNRAS, 282, L53
 Matt, G., Perola, G. C., & Piro, L. 1991, A&A, 247, 25
 Nandra, K., George, I. M., Mushotzky, R. F., Turner, T. J., & Yaqoob, T. 1997, ApJ, 477, 602
 Peterson, B. M., et al. 1999, ApJ, 510, 659
 Reynolds, C. S., & Begelman, M. C. 1997, ApJ, 488, 109
 Reynolds, C. S., Young, A. J., Begelman, M. C., & Fabian, A. C. 1999 (R99), ApJ, 514, 164
 Stella, L. 1990, Nature, 344, 747
 Tanaka, Y., et al. 1995, Nature, 375, 659
 Young, A. J., Ross, R. R., & Fabian, A. C. 1998, MNRAS, 300, L11

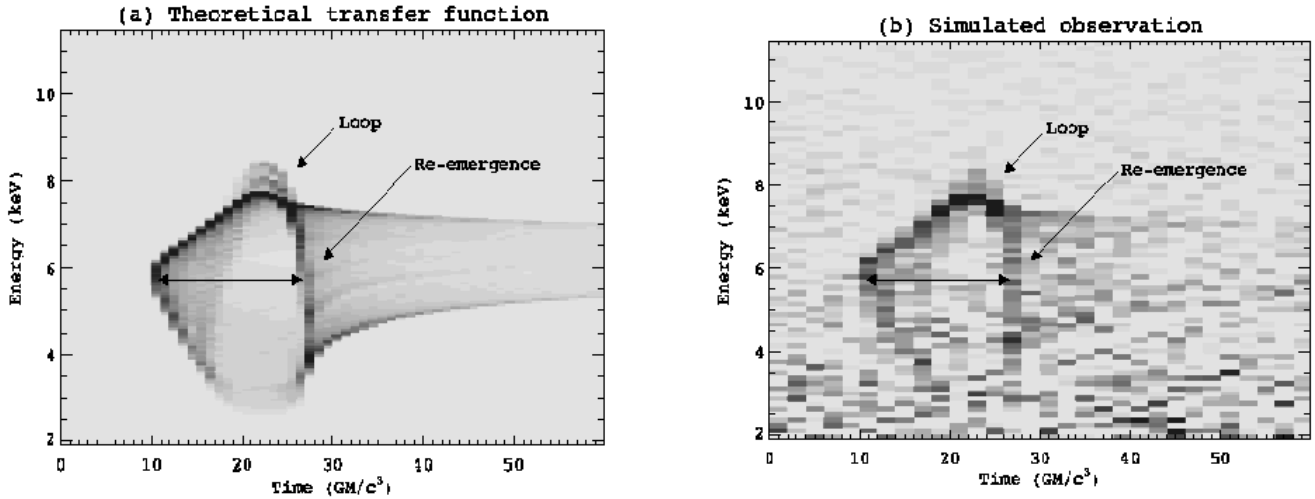


Fig. 6.— Panel (a) shows the theoretical transfer function for a Schwarzschild case with an inclination of 60° and an on-axis flare at a height of $10GM/c^2$. Note the ‘loops’ in the transfer function corresponding to fluorescence from the ionized regions of the disk within the innermost stable orbit. The horizontal line shows the time delay between the initial response and the ‘re-emergence’ which may be used to estimate the black hole mass. Panel (b) shows the simulated observed transfer function. The loops are still visible. The data have been rebinned to produce these figures with improved signal-to-noise ratio.

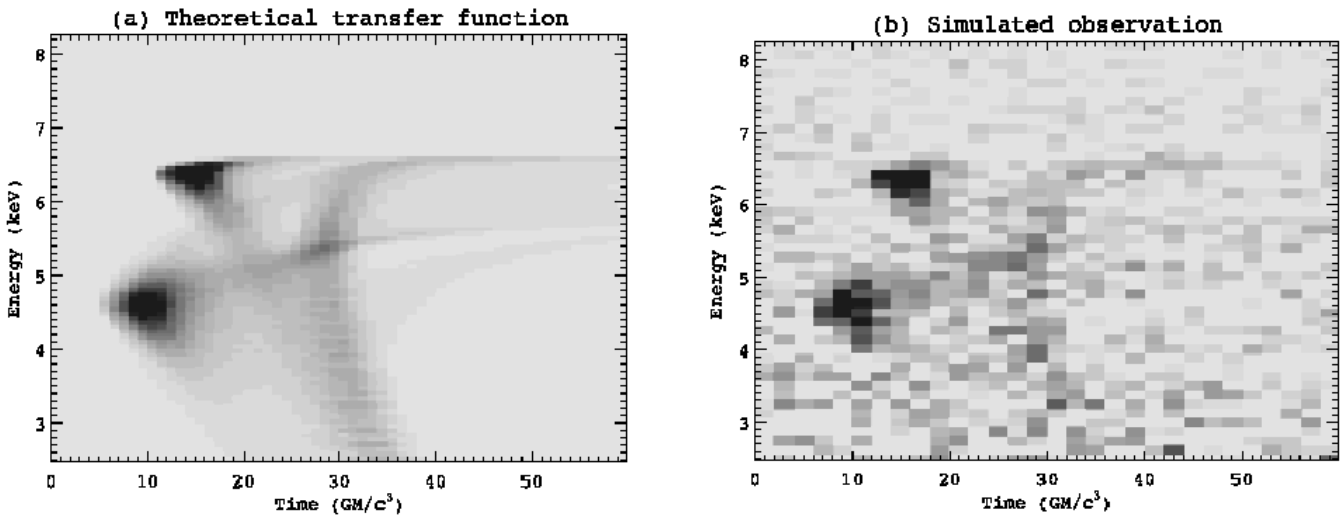


Fig. 7.— Panel (a) shows the theoretical line response to the two overlapping flares described in the text. Panel (b) shows the simulated line response as seen by *Constellation-X*. The individual transfer functions of the two flares can be discerned. The data have been rebinned to produce these figures with improved signal-to-noise ratio.